The Cryosphere Discuss., 6, 3349–3367, 2012
www.the-cryosphere-discuss.net/6/3349/2012/
doi:10.5194/tcd-6-3349-2012

The Cryosphere Discussions

Variability of sea ice deformation rates in the Arctic and their relationship with basin-scale wind forcing

A. Herman and O. Glowacki

Institute of Oceanography, University of Gdańsk, Pilsudskiego 46, 81–378 Gdynia, Poland

Received: 24 July 2012 – Accepted: 26 July 2012 – Published: 9 August 2012

Correspondence to: A. Herman (oceagah@ug.edu.pl)

Published by Copernicus Publications on behalf of the European Geosciences Union.

Abstract

In this paper, temporal variability of the moments of probability distribution functions (pdfs) of total sea ice deformation rates in the Arctic is analyzed in the context of the basin-scale wind forcing acting on the ice. The pdfs are estimated for 594 satellite-derived sea ice deformation maps from 11 winter seasons between 1996/1997 and 2007/2008, provided by the RADARSAT Geophysical Processor System. The moments of the pdfs, calculated for a range of spatial scales, have two dominating components of variability: a seasonal cycle, with deformation rates decreasing throughout winter towards a minimum in March; and a short-term, synoptic variability, strongly correlated with the area-averaged magnitude of the wind stress over the Arctic, estimated based on the NCEP-DOE Reanalysis-2 data (correlation coefficient of 0.71 for the mean deformation rate). Due to scaling properties of the moments, logarithms of higher moments are strongly correlated with the wind stress as well. By demonstrating that a very simple model can provide an explanation for the observed relationships, we show that they reflect the dominating balance of forces in the compact, quasi-stationary ice pack. Finally, we suggest that a positive trend in seasonally-averaged correlation between sea ice deformation rates and the wind forcing, present in the analyzed data, may be related to an observed decrease in the multi-year ice area in the Arctic, indicating possibly even stronger correlations in the future.

1 Introduction

Sea ice deformation constitutes an important factor in the evolution of the sea ice cover at all temporal and spatial scales. Through a number of feedbacks and interactions with other processes, it influences ice thickness distribution, its mechanical strength, new ice production and melting, and the ocean–atmosphere heat transport.

Deformation in a compact ice pack occupying the central part of the Arctic basin is highly localized (Schulson, 2004; Stern and Lindsay, 2009). It takes place in narrow,

TCD
6, 3349–3367, 2012

elongated zones separating semi-rigid floes (Fig. 1a, b). Several recent studies, based on satellite data and/or drifting-buoy analysis, have revealed an intermittent, multifractal character of ice deformation (e.g. Weiss, 2001, 2008; Marsan et al., 2004; Weiss and Marsan, 2004; Rampal et al., 2009b; Stern and Lindsay, 2009; Hutchings et al., 2011). Probability distribution functions (pdfs) of deformation rates are heavy-tailed, and their tails can be well approximated by a power law. Different values of the exponents of the power-law tails have been reported, and at present no theory exists that would explain the observed variability of shapes of the pdfs of sea ice deformation rates. The intrinsic features of sea-ice deformation are generally poorly resolved in numerical sea ice models, especially those based on various versions of the viscous-plastic rheology. For example, Girard et al. (2009) showed recently that sea-ice models in which deformation is based on continuum mechanics generally do not reproduce scaling properties of sea-ice deformation. Only recently, successful attempts have been made to incorporate elasto-brittle effects, crucial for long-range damage propagation, in sea ice models (Girard et al., 2011). However, our knowledge concerning the underlying mechanisms governing sea ice deformation still remains far from satisfactory.

Relationships between sea ice motion and deformation on the one hand, and various components of the atmospheric and oceanic forcing on the other hand, have been investigated in a number of studies that searched for statistically relevant correspondence between sets of variables representing the two groups of processes. Among the atmospheric variables analyzed are geostrophic wind speed (Serreze et al., 1989); atmospheric circulation indices, e.g. the Arctic Oscillation (Kwok, 2006; Rampal et al., 2009a; Comiso, 2012); sea surface pressure distribution (Asplin et al., 2009; Kwok and Cunningham, 2011); or the number, intensity and tracks of cyclones over the Arctic, and the related cloud cover (Screen et al., 2011). The conclusions from those studies strongly depend on the type of data used (satellite, buoys, etc.), the temporal and spatial scale of the analysis, and the study period, underlining the very complicated nature of relationships and feedbacks between the atmosphere, ocean and ice processes involved.

The goal of this paper is twofold. Firstly, we want to analyze temporal variability of the properties of pdfs of observed sea ice deformation rates at temporal scales of a few days and at spatial scales from tens to hundreds of kilometers. Secondly, we want to gain insight into relationships between the wind forcing acting on the ice and ice deformation rates. To this end, we analyze short-term, synoptic variability of satellite-derived sea ice deformation rates in the Arctic basin in the context of, arguably, one of the simplest atmospheric variables thinkable, namely the area-averaged magnitude of the wind stress, calculated from the 10-m wind speed over the Arctic basin. We demonstrate that, regardless of the fact that by performing area-averaging we lose all information on the spatial variability of the wind field, the mean wind stress still explains a substantial part of the variance of sea ice deformation rates. In the last part of the paper, we show that a very simple model provides an explanation for the observed relationships.

The paper is structured as follows: the next section contains a brief description of the data and the statistical methods used. The results of the analysis are presented in Sect. 3, followed by a discussion and conclusions in Sect. 4.

2 Data and methods

2.1 Sea ice deformation and wind data

In this work, we use the RADARSAT Geophysical Processor System (RGPS) sea ice data from the Synthetic Aperture Radar (SAR) imagery of the Arctic Ocean, provided by the RADARSAT-1 satellite. The available products include the ice motion, obtained with a feature-tracking procedure of Kwok et al. (1990). The RGPS products have a temporal resolution of 3 days. The data are available in two versions: in a Lagrangian form, as well as processed onto a regular grid in a polar stereographic projection, with a constant spatial resolution $\Delta x = 12.55$ km (see

TCD
6, 3349–3367, 2012

http://rkwok.jpl.nasa.gov/radarsat/3daygridded.html). In this work, we use the gridded RGPS fields of the shear rate $\dot{\epsilon}_\mathrm{s}$, and the divergence rate $\dot{\epsilon}_\mathrm{d}$, defined as:

$$\dot{\epsilon}_\mathrm{d} = \frac{\partial u}{\partial x} + \frac{\partial v}{\partial y}, \quad \dot{\epsilon}_\mathrm{s} = \left[\left(\frac{\partial u}{\partial x} - \frac{\partial v}{\partial y}\right)^2 + \left(\frac{\partial u}{\partial y} + \frac{\partial v}{\partial x}\right)^2\right]^{1/2} \tag{1}$$

where u, v denote the velocity components along the x and y axis of the regular grid, respectively. At present, the available data cover 11 winter seasons (November–April) from 1996/1997 to 2007/2008 (except 2002/2003). Data from summer periods are not used in this study.

The daily 10-m wind speed data come from the NCEP-DOE Reanalysis 2 data set (Kanamitsu et al., 2002). The data are available on a global grid with a spatial resolution 1.875° longitude and 1.904° latitude.

2.2 Data preprocessing and analysis

Our analysis is limited to the total deformation rate $\dot{\epsilon}_\mathrm{t}$, which is a scalar quantity defined as (e.g. Girard et al., 2009):

$$\dot{\epsilon}_\mathrm{t} = \left(\dot{\epsilon}_\mathrm{s}^2 + \dot{\epsilon}_\mathrm{d}^2\right)^{1/2}. \tag{2}$$

We calculated the moments $m_{q,L}$ of the pdfs of $\dot{\epsilon}_\mathrm{t}$ for a range of spatial scales $L = n\Delta x$, starting from the original mesh size Δx ($n = 1$) up to 916 km ($n = 73$), and for the power q ranging from 0.5 to 3.0:

$$m_{q,L} = \left\langle \dot{\epsilon}_{\mathrm{t},L}^{q} \right\rangle, \tag{3}$$

where $\langle\cdot\rangle$ denotes averaging over all grid cells of a given deformation-rate map with resolution L (Fig. 1c). The maps with resolution lower than Δx, i.e. for $n > 1$, were obtained by averaging of the original data within $n \times n$ windows and removing meshes containing less than $n^2/2$ data points. After removal of maps with very large amount of gaps, a total of $N = 594$ maps have been retained for further analysis, each with at least 1.2×10^4 data points.

The magnitude of wind stress τ_a was calculated from the 10-m wind speed U_{10} as $\tau_a = \rho_a C_D U_{10}^2$, assuming a constant air density $\rho_a = 1.27\,\mathrm{kg\,m^{-3}}$ and an air-ice drag coefficient $C_D = 2 \times 10^{-3}$. The time series of basin-averaged wind stress $\bar{\tau}_a = \bar{\tau}_a(t)$ was obtained by averaging within the region marked in Fig. 1 and over three-day periods leading the corresponding time windows of the RGPS data by $\Delta t = 2$ days. To account for variable spatial resolution of the NCEP/DOE data, the values of τ_a were interpolated onto the regular RGPS grid before averaging. The optimal value of Δt was selected based on a preliminary analysis of correlation coefficients between $\bar{\tau}_a$ and logarithms of $m_{q,L}$ (see further).

All correlation coefficients reported in the remaining part of this paper were calculated with a bootstrap method by averaging over 1000 random sub-samples of the original datasets, each containing 99 % of all data points. Cubic-spline functions were used to estimate nonlinear trends in the ice deformation data.

3 Results

Figure 1 shows two representative examples of sea ice deformation rate maps from the analyzed data set. As is already known (see, e.g. Marsan et al., 2004; Hutchings et al., 2011), deformation rates have multifractal properties, with:

$$m_{q,L} \sim L^{-\beta(q)}, \tag{4}$$

where β is a positive, increasing, convex function of q. For mean sea ice deformation rates ($q = 1$) in the Arctic, β is close to 0.2 (Marsan et al., 2004), although it exhibits a clear seasonal cycle with highest values during the summer (Stern and Lindsay, 2009). Generally, deviations from the scaling relationship occur only for higher moments ($q > 2$) and small spatial scales during short episodes of strong deformation, like the one shown in Fig. 1a, c. Similarly to the exponent β, the mean intensity of sea ice deformation reveals a pronounced seasonal and short-term time variability, reflecting the state of the ice cover and the forcing acting on it.

Let us introduce the notation: $\tilde{m}_{q,L} \equiv \log_{10} m_{q,L}$. Obviously, from the scaling relationship Eq. (4) it follows that:

$$\tilde{m}_{q_1,L_2} = \tilde{m}_{q_1,L_1} - \beta(q_1)\log_{10}(L_2/L_1) \tag{5}$$

and

$$\tilde{m}_{q_2,L_1} \sim \frac{\beta(q_2)}{\beta(q_1)}\tilde{m}_{q_1,L_1}, \tag{6}$$

i.e. the relationship between the logarithms of the moments at different scales L and for different powers q is linear.

In the following, the correlation coefficient between $\bar{\tau}_a$ and $\tilde{m}_{q,L}$ will be denoted with $C = C(q,L)$. As mentioned in Sect. 2.2, the values of C are highest for a time lag Δt between the two data sets equal 2 days (presumably, the optimal value of Δt is smaller in weaker first-year ice, reacting faster to changes of the external forcing, than in thick and strong multi-year ice; however, as this study concentrates on the basin-scale forcing and sea ice deformation, this supposed spatial variability of the characteristic reaction time of the ice cover to the forcing is not taken into account and Δt is set constant). Figure 2a shows a scatter plot of the data for $q = 1$ and $L = \Delta x$ (scatter plots for other (q,L)-combinations are similar). As expected, the deformation rates increase with increasing wind forcing, with $C = 0.61$ for the mean deformation rate ($q = 1$) and slightly lower values for higher moments (not shown). However, the distribution of the data points reveals an interesting seasonal pattern of sea ice deformation. The same mean wind stress tends to be associated with higher deformation rates at the beginning of the winter season (November–December) than in late winter and early spring (March–April). A seasonal cycle, with a tendency of the mean deformation rates to decrease from November to March, is clearly visible in the time series of $\tilde{m}_{q,L}$, shown in Fig. 3a for the 1999/2000 winter, and in the Supplement Fig. 1 for the remaining winter seasons. Although a strong inter-annual variability is present, nonlinear trend lines fitted to the data within individual seasons generally have a minimum in March, coinciding with the maximum thickness and extent of the ice cover. The trend changes sign in April, with the onset of the melting season. Not surprisingly, this intra-seasonal variability is in agreement with the annual cycle of the mean monthly shear rates reported by Kwok (2006) and Kwok and Cunningham (2011), as well as the annual cycle of mean deformation rates obtained by Stern and Lindsay (2009), who used the Lagrangian RGPS data. Similarly, there is a clear annual minimum in March in drifting-buoy-derived sea ice speeds calculated by Rampal et al. (2009a). Strong seasonal variability in mechanical behavior of the Arctic sea ice has been also found by Gimbert et al. (2012), who analyzed changes of the inertial motion intensity in the Arctic.

The correlation coefficients C, recalculated for seasonally-detrended data, are significantly higher than those obtained for the original time series (Figs. 2b and 3b). Generally, if the deformation data exhibited perfect scaling, $C(q,L)$ would be constant due to linear relationship Eqs. (5) and (6). Thus, the variability of $C(q,L)$, shown in Fig. 4, mirrors the deviations from the scaling properties of the moments. For instance, for low values of q the deviations from scaling are small (Fig. 1c), and hence no strong dependence of C on L can be observed, with C decreasing slowly with L from 0.71 to 0.68. Lower, but still statistically significant (at a 99 % confidence level) values of C occur only for high moments and small length scales, i.e. for (q,L)-combinations for which the largest deviations from scaling Eq. (6) are present – which is not surprising considering that those (q,L)-pairs represent mainly very strong, localized deformation events that may be decoupled from the overall large-scale deformation pattern resulting from the basin-scale wind forcing.

TCD
6, 3349–3367, 2012

Arctic sea ice deformation rates

A. Herman and O. Glowacki

4 Discussion and conclusions

The use of the surface wind stress, i.e. a quantity directly determining forcing acting on the ice – as opposed to other variables, e.g. the atmospheric pressure or upper-level winds, used in a number of other studies – seems particularly appropriate for the analysis of atmosphere–sea ice relationships on short time scales. This is especially true in winter, when, due to high vertical stability of the lower troposphere (e.g. Devasthale et al., 2010), there is no close coupling between the boundary-layer and free-troposphere winds. Seasonally varying momentum transfer between the atmosphere and sea ice has been identified previously as one of the causes of the existence of a seasonal cycle in ice deformation (Kwok, 2006). This decoupling may partly explain low correlation between sea ice deformation and indices of large-scale atmospheric circulation reported by some authors (e.g. Rampal et al., 2009a). As argued recently by Tsukernik et al. (2010), sufficient explanation of sea ice–atmosphere interactions may require accounting for processes acting on time scales shorter than monthly or seasonal.

The results described in this work suggest the existence of two important components of variability of sea ice deformation rates in the Arctic. The first is the annual cycle (Fig. 3a and Supplement Fig. 1), which does not have a relationship with wind forcing, but reflects seasonal changes of the properties of the ice cover itself – its thickness, compactness, mechanical strength and, importantly, ice-extent related degree of confinement by the basin's boundaries. The second component is the (sub)synoptic variability related – directly or indirectly via other processes – to the wind stress acting on the ice (Fig. 3b). Obviously, high lagged correlation between two time series does not imply causality. However, in the analyzed case, the observed relationships can be explained with a simple, quasi-static model, similar to the one used by Girard et al. (2011). Let us assume that in a compact ice cover there is a balance between the forcing term **F**, proportional to $-\bar{\tau}_a$, and the internal stress term:

$$\nabla \cdot \boldsymbol{\sigma} + \mathbf{F} = 0. \tag{7}$$

TCD
6, 3349–3367, 2012

Further, let us use a simple, linear rheology model, $\boldsymbol{\sigma} = J\boldsymbol{\epsilon}_\mathrm{t}$, where J is a (spatially variable) measure of the strength of the ice and $\boldsymbol{\epsilon}_\mathrm{t}$ denotes strain. (It is worth noticing that in the RGPS data we have simply $\epsilon_\mathrm{t} = \dot{\epsilon}_\mathrm{t}\delta t$ with δt equal 3 days.) For simplicity, we will solve the model numerically in a one-dimensional (1-D) case; an extension to 2 dimensions is straightforward and leads to the same conclusions, but requires more lengthy calculations. We define a 1-D domain composed of $i = 1, \ldots, N_x$ square boxes of size L. The forcing F_i is applied to the center of each box, and deformation $\epsilon_{\mathrm{t},i,i+1}$ takes place at the joints between neighboring boxes, having strength $J_{i,i+1}$. For the i-th box we have from Eq. (7):

$$(J_{i,i+1}\epsilon_{\mathrm{t},i,i+1} - J_{i-1,i}\epsilon_{\mathrm{t},i-1,i}) + LF_i = 0.$$

By integrating iteratively from the left boundary, we obtain:

$$\epsilon_{\mathrm{t},i,i+1} = \frac{J_{0,1}}{J_{i,i+1}}\epsilon_{\mathrm{t},0,1} - \frac{L}{J_{i,i+1}}\sum_{j=1}^{i} F_j.$$

If we assume that J and F are independent random variables, the average deformation $m_{1,L}$ can be written as:

$$m_{1,L} = \overline{J^{-1}}\left(J_{0,1}\epsilon_{\mathrm{t},0,1} - \frac{LN_x}{2}\overline{F}\right), \tag{8}$$

where bars denote averages over the model domain.

Thus, in this simplified model, a linear relationship between the area-averaged wind stress and the mean sea ice deformation rate is a direct consequence of the assumptions listed above.

Returning to the RGPS data analyzed in this paper, it must be first noticed that the range of values of $m_{1,L}$ (between 0.003 and 0.044 day^{-1}) is small enough so that $\tilde{m}_{1,L}$ can be approximated as a linear function of $m_{1,L}$ – the respective correlation coefficient equals 0.965, and correlation between $\bar{\tau}_a$ and $m_{1,L}$ equals 0.73. The reason for using the logarithm $\tilde{m}_{1,L}$ instead of non-logarithmed values of $m_{1,L}$, was a consistency of the treatment of all moments, for which the scaling relationship Eqs. (5) and (6) are expected to hold.

Thus, high correlation between $\bar{\tau}_a$ and $m_{1,L}$ obtained in this study indicates that Eq. (7) correctly describes the leading-order balance of forces in the Arctic sea ice, i.e. the dominant basin-scale forcing acting on the ice is due to wind (and, presumably, wind-driven currents, directly correlated to the wind stress). As already noticed, high correlation coefficients with logarithms of the higher moments and larger length scales, $q > 1$ and $L > \Delta x$, are a direct result of the scaling properties of deformation.

Finally, it is interesting to note a slightly positive trend in correlation between the wind forcing and sea ice deformation rates, calculated separately for individual winter seasons within the analysis period (Fig. 5). Obviously, 11 data points are far from sufficient for any statistics. Nevertheless, it is tempting to hypothesize that this trend is related to the recent decrease in the multi-year ice area in the Arctic (Comiso, 2012). Deformation rates are generally higher in seasonal, relatively weak and thin ice than in the thick, multi-year ice. First-year ice is expected to respond more directly to the wind forcing, and hence, its increasing amount may lead to higher basin-scale wind stress–ice deformation correlations. Thus, higher sea ice deformation rates are expected for those winters, for which particularly strong melting occurred in the preceding summer and autumn periods. Interestingly, within the period of study there were 3 local minima in the November multi-year ice area, as estimated by Comiso (2012) – in 1999, 2007, and, less pronounced, in 2003. They correspond to the peaks in seasonally-averaged values of C in the following winters (Fig. 5), with the correlation coefficient for $q = 1$ approaching a remarkably high value of 0.9 in the 2007/2008 winter, after the record ice minimum in the summer of 2007. Another indication of longer-term processes may be a change in the seasonal cycle of deformation that occurred during the analysis period. Comparison of the trend lines shown in Supplement Fig. 1 clearly shows that the March minimum of deformation rates has become shallower, i.e. the winter-time negative trend in deformation rates has decreased (only 2 winters, 1997/1998 and 2005/2006, show an exception from this tendency). It may be a consequence of the thinning of the ice cover, which is becoming more susceptible to deformation even during the maximum annual sea ice extent and thickness. This notion is supported by the results of a recent study by Gimbert et al. (2012) who observed a positive trend in the inertial-motion intensity in the Arctic over the last decade and interpreted it as a consequence of a mechanical weakening of the ice cover. More data covering a longer time period will be necessary to verify the statistical significance of those trends.

Supplementary material related to this article is available online at: http://www.the-cryosphere-discuss.net/6/3349/2012/tcd-6-3349-2012-supplement.pdf.

Acknowledgements. NCEP Reanalysis 2 data were provided by the NOAA/OAR/ESRL PSD, Boulder, Colorado, USA, from their web site at http://www.esrl.noaa.gov/psd/. RGPS data are made available by the Jet Propulsion Laboratory at http://rkwok.jpl.nasa.gov/radarsat/index.html.

References

Asplin, M., Lukovich, J., and Barber, D.: Atmospheric forcing of the Beaufort Sea ice gyre: surface pressure climatology and sea ice motion, J. Geophys. Res., 114, C00A06, doi:10.1029/2008JC005127, 2009. 3351

Comiso, J.: Large decadal decline of the Arctic multiyear ice cover, J. Climate, 25, 1176–1193, 2012. 3351, 3359

Devasthale, A., Willéen, U., Karlsson, K.-G., and Jones, C. G.: Quantifying the clear-sky temperature inversion frequency and strength over the Arctic Ocean during summer and winter seasons from AIRS profiles, Atmos. Chem. Phys., 10, 5565–5572, doi:10.5194/acp-10-5565-2010, 2010. 3357

Gimbert, F., Jourdain, N., Marsan, D., Weiss, J., and Barnier, B.: Recent mechanical weakening of the Arctic Sea ice cover as revealed from larger inertial oscillations, J. Geophys. Res., 117, C00J12, doi:10.1029/2011JC007633, 2012. 3356, 3360

Girard, L., Weiss, J., Molines, J., Barnier, B., and Bouillon, S.: Evaluation of high-resolution sea ice models on the basis of statistical and scaling properties of Arctic Sea ice drift and deformation, J. Geophys. Res., 114, C08015, doi:10.1029/2008JC005182, 2009. 3351, 3353

Girard, L., Bouillon, S., Weiss, J., Amitrano, D., Fichefet, T., and Legat, V.: A new modeling framework for sea-ice mechanics based on elasto-brittle rheology, Ann. Glaciol., 52, 123–132, 2011. 3351, 3357

Hutchings, J., Roberts, A., Geiger, C., and Richter-Menge, J.: Spatial and temporal characterization of sea-ice deformation, Ann. Glaciol., 52, 360–368, 2011. 3351, 3354

Kanamitsu, M., Ebisuzaki, W., Woollen, J., Yang, S.-K., Hnilo, J., Fiorino, M., and Potter, G.: NCEP–DOE AMIP-II reanalysis (R-2), B. Am. Meteorol. Soc., 11, 1631–1643, doi:10.1175/BAMS-83-11-1631, 2002. 3353

Kwok, R.: Contrasts in sea ice deformation and production in the Arctic seasonal and perennial ice zones, J. Geophys. Res., 111, C11S22, doi:10.1029/2005JC003246, 2006. 3351, 3356, 3357

Kwok, R. and Cunningham, G.: Deformation of the Arctic Ocean ice cover after the 2007 record minimum in summer ice extent, Cold Reg. Sci. Technol., 76–77, 17–23, 2011. 3351, 3356

Kwok, R., Curlander, J., McConnell, R., and Pang, S.: An ice-motion tracking system at the Alaska SAR facility, IEEE J. Oceanic Eng., 15, 44–54, 1990. 3352

Marsan, D., Stern, H., Lindsay, R., and Weiss, J.: Scale dependence and localization of the deformation of Arctic Sea ice, Phys. Rev. Lett., 93, 178501, doi:10.1103/PhysRevLett.93.178501, 2004. 3351, 3354

Rampal, P., Weiss, J., and Marsan, D.: Positive trend in the mean speed and deformation rate of Arctic Sea ice, 1979–2007, J. Geophys. Res., 114, C05013, doi:10.1029/2008JC005066, 2009a. 3351, 3356, 3357

Rampal, P., Weiss, J., Marsan, D., and Bourgoin, M.: Arctic sea ice velocity field: general circulation and turbulent-like fluctuations, J. Geophys. Res., 114, C10014, doi:10.1029/2008JC005227, 2009b. 3351

Schulson, E.: Compressive shear faults within arctic sea ice: fracture on scales large and small, J. Geophys. Res., 109, C07016, doi:10.1029/2003JC002108, 2004. 3350

TCD
6, 3349–3367, 2012

Arctic sea ice deformation rates

A. Herman and O. Glowacki

Screen, J., Simmonds, I., and Keay, K.: Dramatic interannual changes of perennial Arctic Sea ice linked to abnormal summer storm activity, J. Geophys. Res., 116, D15105, doi:10.1029/2011JD015847, 2011. 3351

Serreze, M., Barry, R., and McLaren, A.: Seasonal variations in sea ice motion and affects on sea ice concentration in the Canada Basin, J. Geophys. Res., 94, 10955–10970, 1989. 3351

Stern, H. and Lindsay, R.: Spatial scaling of Arctic Sea ice deformation, J. Geophys. Res., 114, C10017, doi:10.1029/2009JC005380, 2009. 3350, 3351, 3354, 3356

Tsukernik, M., Deser, C., Alexander, M., and Thomas, R.: Atmospheric forcing of Fram Strait sea ice export: a closer look, Clim. Dynam., 35, 1349–1360, doi:10.1007/s00382-009-0647-z, 2010. 3357

Weiss, J.: Fracture and fragmentation of ice: a fractal analysis of scale invariance, Eng. Fract. Mech., 68, 1975–2012, 2001. 3351

Weiss, J.: Intermittency of principal stress directions within Arctic Sea ice, Phys. Rev. E, 77, 056106, doi:10.1103/PhysRevE.77.056106, 2008. 3351

Weiss, J. and Marsan, D.: Scale properties of sea ice deformation and fracturing, C. R. Phys., 5, 735–751, 2004. 3351

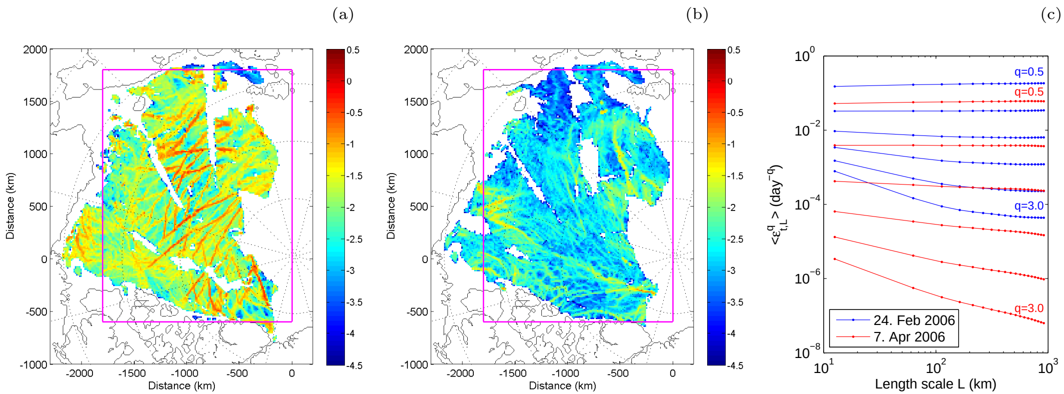

Fig. 1. Total sea ice deformation rate $\dot{\epsilon}_t$ in the Arctic on 24 February ($\bar{\tau}_a = 0.24\,N\,m^{-2}$) and 7 April 2006 ($\bar{\tau}_a = 0.03\,N\,m^{-2}$): maps of $\dot{\epsilon}_t$ (in day^{-1}), shown in a logarithmic color scale **(a)**, **(b)**; and moments $m_{q,L}$ for a range of length scales L and powers q **(c)**. The boxes in **(a)**, **(b)** show the area within which $\bar{\tau}_a$ was calculated. The lines in **(c)** are drawn for q increasing from 0.5 to 3.0 with a step of 0.5.

TCD
6, 3349–3367, 2012

Arctic sea ice deformation rates

A. Herman and O. Glowacki

Title Page
Abstract | Introduction
Conclusions | References
Tables | Figures
◀| |▶
◀ ▶
Back | Close
Full Screen / Esc
Printer-friendly Version
Interactive Discussion

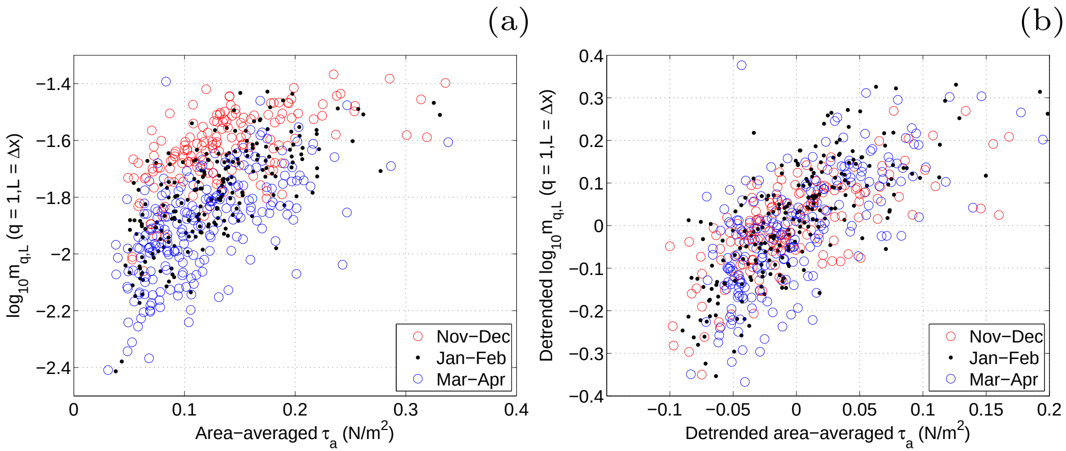

Fig. 2. Scatter plots of $\tilde{m}_{q,L}$ (for $q = 1$ and $L = \Delta x$) against $\bar{\tau}_a$ for the original, **(a)** $C = 0.61$, and seasonally-detrended, **(b)** $C = 0.71$, data from the whole analysis period 1996–2008.

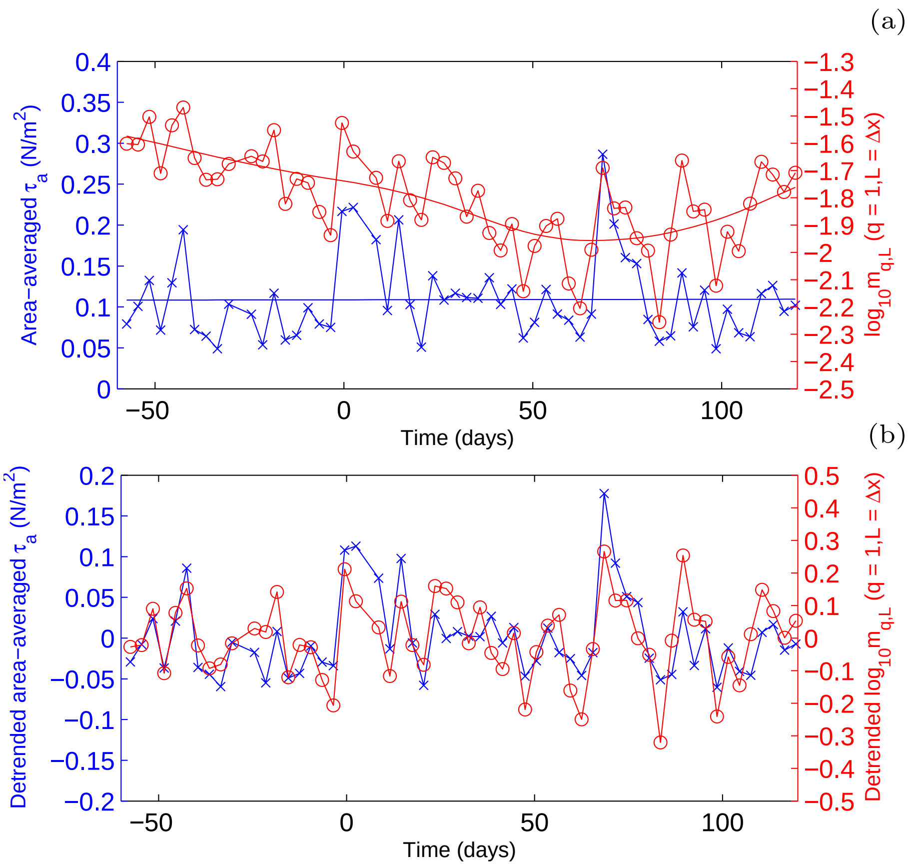

Fig. 3. Time series of $\bar{\tau}_a$ ($N\,m^{-2}$) and $\tilde{m}_{q,L}$ (for $q = 1$ and $L = \Delta x$) in the 1999/2000 winter: original data with trend lines **(a)** and detrended data **(b)**. Time is shown in days after 1 January 2000. See Supplement Fig. 1 for other winter seasons.

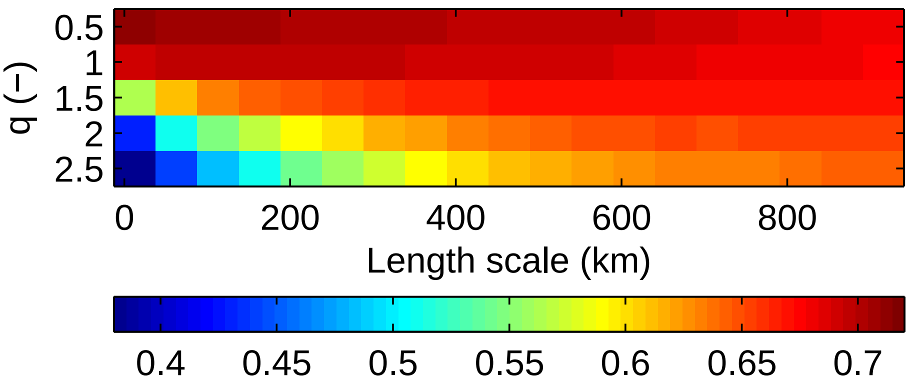

Fig. 4. Variability of the correlation coefficient $C(q,L)$ between $\bar{\tau}_a$ and $\tilde{m}_{q,L}$, calculated for seasonally-detrended data from the whole data set.

TCD
6, 3349–3367, 2012

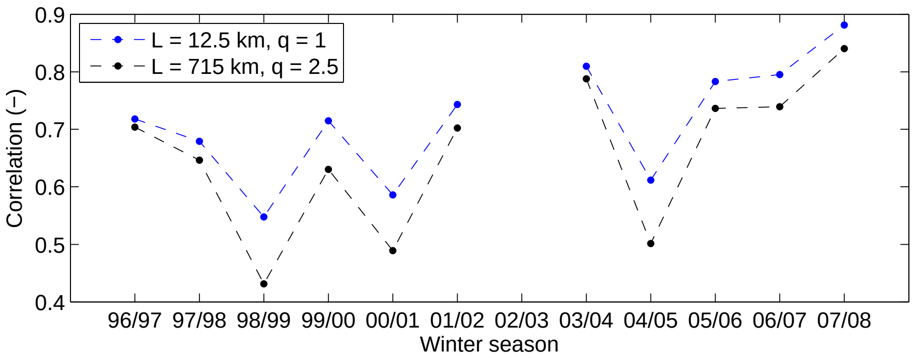

Fig. 5. Inter-annual variability of C in the study period for two selected (q, L)-pairs, calculated for seasonally-detrended data.